Available online at www.sciencedirect.com
ScienceDirect
Journal of the European Ceramic Society 30 (2010) 793–798
www.elsevier.com/locate/jeurceramsoc

Technical note

WC-reinforced (Ti,W)(CN)

Youngjae Kang [a], Shinhoo Kang [b,*]

[a] High Voltage Electron Microscopy Station, National Institute for Materials Science, Tsukuba 305-0005, Japan
[b] Department of Materials Science and Engineering, Seoul National University, Seoul 151-744, Republic of Korea

Received 30 April 2009; received in revised form 27 August 2009; accepted 10 September 2009
Available online 9 October 2009

Abstract

A ceramic microstructure of WC-reinforced (Ti,W)(CN) was designed using thermodynamic instability among the constituent elements and gas species involved in the sintering process. During sintering WC in the shape of platelets formed in (Ti,W)(CN) solid-solution ceramics, which were synthesized from milled mixtures of oxides with carbon. The WC platelets separated from the (Ti,W)(CN) ceramics due to the low chemical affinity of tungsten for nitrogen. The shape of WC varies depending on the composition of the binder phase and the sintering conditions. With increasing binder content, the WC platelet shape became more irregular. This change was attributed not only to surface energy but also to the formation mechanism. The presence of WC platelets toughened (Ti,W)(CN) significantly at excellent hardness value (H_v: 18.5–20.0 GPa, K_{IC}: 6.0–6.8 MPa $m^{1/2}$) as compared to those of recently reported advanced structural ceramics.

Keywords: (Ti,W)(CN); Platelets; Microstructure; Toughness and toughening; Cutting tools

1. Introduction

TiC- and Ti(CN)-based cermets demonstrate excellent hardness, thermal stability at high temperatures, and resistance to deformation, wear, and corrosion.[1] These cermets typically have a core–rim structure. Recently, Ti-based solid-solution cermets showed highly attractive mechanical properties.[2] (Ti,W)(CN)-based solid-solution carbides in particular exhibit improved hardness and indentation toughness over conventional TiC-based cermets and other structural ceramics.[3–8] The synthesis of (Ti,W)(CN) powders, through high-energy ball milling and carbothermal reduction of oxide mixtures, is well described elsewhere.[9–12] The presence of the metallic phase, which was introduced from the milling media, enabled the densification of (Ti,W)(CN) at low temperatures without external pressure.

Whiskers and platelets in ceramic microstructures increase fracture toughness by inducing crack deflection and crack bridging.[13–15] Often in cemented carbides, large WC grains appear in the microstructure due to abnormal grain growth.[16–19] The mechanism for abnormal WC growth is well described in the literature.[20] Sometimes WC platelets have been added intentionally to serve as seed crystals during powder metallurgy processes.[21,22] It has been shown that ribbon-shaped WC particles precipitate in $(W_{0.75}Ti_{0.25})C$ during quenching and annealing.[23] These processes require high temperatures.[24]

In this study WC thin platelets with large aspect ratios (>20) formed in (Ti,W)(CN) during sintering. We also investigated the dependence of the microstructure changes in (Ti,W)(CN)-based carbides on the binder content and processing conditions during sintering. The mechanical properties of (Ti,W)(CN) were strongly dependent on its microstructures.

2. Experimental procedures

The starting materials, viz. anatase-TiO_2, WO_3 and C powders, were mixed to produce the nominal composition of $(Ti_{1-x}W_x)C$-yMe (y = 0–20 wt%), where the mole fraction, x, was varied from 0.30 to 0.50. The targeted compositions were $(Ti_{0.7}W_{0.3})C$, $(Ti_{0.6}W_{0.4})C$, and $(Ti_{0.5}W_{0.5})C$ and they were renamed as $(Ti_{1-x}W_x)(CN)$ after sintering in a nitrogen atmosphere. The mixed powders were then subjected to high-energy ball milling using a planetary mill (Fritsch Pulverisette 5). Tungsten carbide balls were used as milling media with a ball-to-

* Corresponding author. Tel.: +82 2 880 7167; fax: +82 2 884 1413.
E-mail address: shinkang@snu.ac.kr (S. Kang).

0955-2219/$ – see front matter © 2009 Elsevier Ltd. All rights reserved.
doi:10.1016/j.jeurceramsoc.2009.09.013

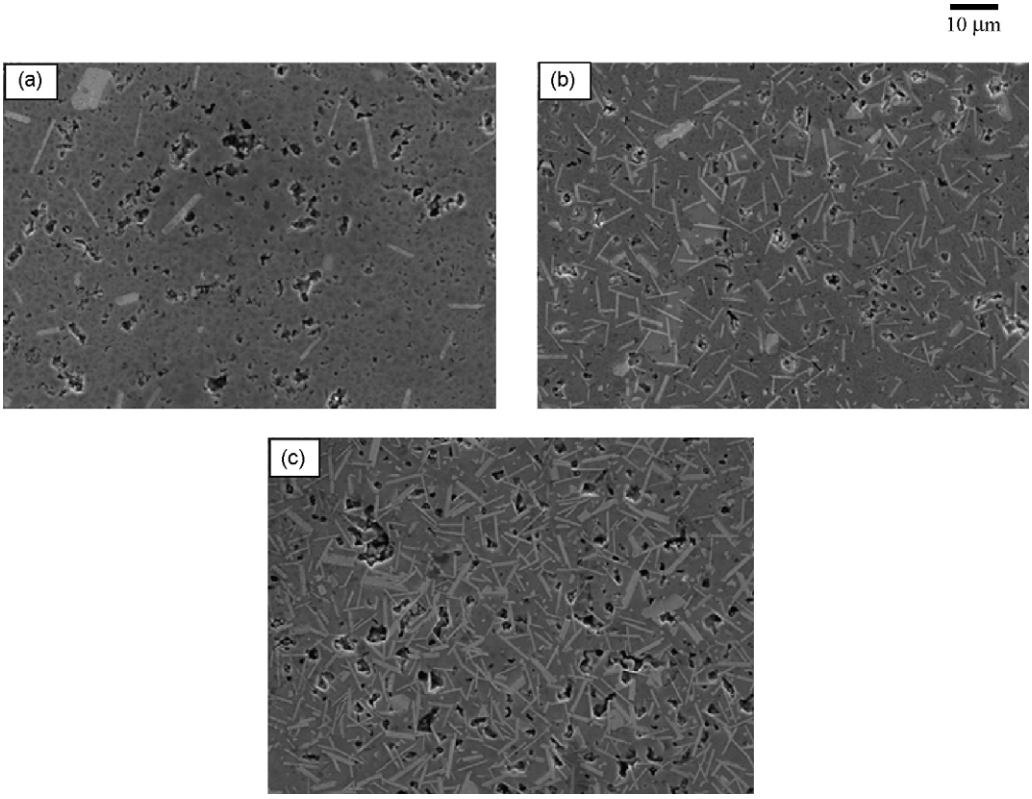

Fig. 1. Microstructure of (Ti,W)(CN) sintered at 1510 °C for 1 h in N_2 at 40 Torr: (a) $(Ti_{0.7}W_{0.3})(CN)$, (b) $(Ti_{0.6}W_{0.4})(CN)$, and (c) $(Ti_{0.5}W_{0.5})(CN)$.

powder weight ratio of 40:1. We used a tungsten carbide-coated bowl. All millings were conducted at a speed of 250 rpm for a period of 20 h. The milled powders were reduced and carburized in a vacuum at 1200 °C for 1 h. The final product of the powders was then compacted at a pressure of 125 MPa. The compacts were then sintered at 1510 °C for 1 h in a vacuum ($\sim 10^{-5}$ MPa) or in a nitrogen atmosphere at pressures of 5, 30 and 40 Torr (1 Torr $\sim 1.33 \times 10^{-4}$ MPa). Nitrogen was introduced throughout sintering (above 1200 °C). Sinter/HIP was also carried out at 1450 °C for 1 h under an argon gas pressure of 8 MPa after pre-sintering at 1350 °C for 1 h to produce fully densified (Ti,W)(CN).

Cross-sectioned specimens were ground with a diamond wheel and then polished from 6 to 1 μm with diamond slurry for microstructure analysis. Microstructures were observed in a scanning electron microscope SEM (JSM-5600, JEOL) in back-scattered electron BSE mode. The area fractions of various microstructures were measured by an image analyzer (UTHSCSA Image Tool). The chemical composition was determined by X-ray energy dispersive analysis (EDS, INCA) on scanning electron microscope (JSM-6700F, JEOL), inductively coupled plasma atomic emission spectrometry (ICP-AES, OPTIMA 4300DV, PerkinElmer) and CNO analysis (R0-400C, TC-400C, WC-600, LECO). The samples were examined for Vickers hardness, H_v, under the indentation load of 30 kg, and the indentation toughness was calculated from H_v and crack length using the expression derived by Evans and Charles.[25] The porosity of sintered carbides was measured according to ASTM B-276.

3. Results and discussion

3.1. Effect of WC content on the microstructure

Fig. 1 shows SEM microstructures of (Ti,W)(CN) as the WC content was varied from 30 to 50%. All samples were sintered at 1510 °C for 1 h under a nitrogen pressure of 40 Torr. A plate-like phase appeared actively as brighter regions when the WC content exceeded 40 at.%. The gray regions in the SEM images were (Ti,W)(CN) solid-solution grains, while the brighter regions were WC precipitates. The high nitrogen pressure and/or insufficient binder phase were responsible for the pores in the microstructures of the (Ti,W)(CN) systems.

The separation of WC from (Ti,W)(CN) in the presence of nitrogen was attributed to the low chemical affinity between nitrogen and W.[26] The (Ti,W)C solid-solution was reported to retain up to 52 at.% WC based on the result of ThermoCalc at 1500 °C.[27] The WC phase separated out more readily due to the low limit of solubility in TiC in the presence of nitrogen. Based on the SEM-EDS and CNO analyses the matrix compositions in Fig. 1a–c are found to be $(Ti_{0.68}W_{0.32})(C_{0.87}N_{0.10})$, $(Ti_{0.68}W_{0.32})(C_{0.88}N_{0.07})$ and $(Ti_{0.67}W_{0.33})(C_{0.85}N_{0.05})$, respectively, along with WC as shown in Table 1. It means that $(Ti_{0.68}W_{0.32})(C_{0.87}N_{0.07})$ is the approximate phase at equilibrium with WC in this processing condition. It is because the WC phase starts separation from the $(Ti_{0.7}W_{0.3})(CN)$ solid-solution. It also indicates that the solubility limit of WC in (Ti,W)(CN) is $\sim$30 at.% at 1500 °C.

Table 1
Final chemical compositions of (Ti,W)C sintered at 1510 °C for 1 h in N_2 at 40 Torr.

Target composition	Phases present and final composition
$(Ti_{0.7}W_{0.3})C$	$(Ti_{0.68}W_{0.32})(C_{0.87}N_{0.10}) + WC$
$(Ti_{0.6}W_{0.4})C$	$(Ti_{0.68}W_{0.32})(C_{0.88}N_{0.07}) + WC$
$(Ti_{0.5}W_{0.5})C$	$(Ti_{0.67}W_{0.33})\ (C_{0.85}N_{0.05}) + WC$

Table 2
Binder composition of $(Ti_{0.6}W_{0.4})C$–*x*Me (in wt%).

Target composition	Fe	Co	Ni	Total binder
X = 0	1.80	1.15	0.6	3.55
X = 5FeCoNi	2.19	2.21	1.76	6.16
X = 5Ni	1.02	0.92	4.82	6.76
X = 10Ni	1.09	0.42	9.76	11.27
X = 20Ni	0.03	0.62	19.25	19.90

The number of WC platelets of lengths greater than 10 μm was low in $(Ti_{0.7}W_{0.3})(CN)$. It appeared, however, that the faceted WC platelets in this system experienced abnormal growth. WC was reported to grow abnormally after 2D nucleation in the WC–Co system.[28] In the systems with low WC concentrations, the concentration of WC nuclei larger than critical size for growth was also low. They re-dissolve and precipitate onto a large abnormally grown WC.

The volume fraction of WC platelets increased with the WC content in (Ti,W)(CN) and the average length of the platelets was ~8 μm. In the $(Ti_{0.5}W_{0.5})(CN)$ system, the volume fraction of WC platelets approached 30%. It is conceivable that in $(Ti_{0.5}W_{0.5})C$ powders of the target composition, WC can be retained as a separate phase if synthesized below 1500 °C. The XRD analysis showed that the $(Ti_{0.6}W_{0.4})C$ and $(Ti_{0.5}W_{0.5})C$ powders synthesized at 1200 °C were composed of the (Ti,W)C and WC phases.[3,10] The pre-existing WC in the powders might have acted as seed for the growth of the WC platelets.

3.2. Effect of binder phase on the WC morphology

We investigated the effect of the binder composition and their contents on the microstructure, especially of the WC morphology. Fig. 2 shows the microstructures of $(Ti_{0.6}W_{0.4})(CN)$-*x*Me cermets (Me = Ni, Co, Fe) sintered at 1510 °C for 1 h in nitrogen at 5 Torr, where *x* varied from 0 to 20 wt%. Pure Ni or Co–30Fe–30Ni (in wt%) alloy was used as binder phase. The binder compositions of the initial powders are analyzed with an ICP-AES and the results are summarized in Table 2. From this analysis we found that the metallic phase gained from milling process of this study is in the range of 0–2.0 wt%. Most contaminants (0.7–2.0 wt%) are Fe and Co, which are from milling jar and media, as expected. Previously these carbides were reported to contain a metallic binder phase consisting of Ni, Cr, Co, and Fe up to 3.5–5 wt%.[3]

A low nitrogen pressure (5 Torr) was employed to observe the sequence of changes in morphology as a function of binder composition and content. The figure shows that the binder composition affects the shape of WC precipitates at a given nitrogen pressure. The WC morphology also changed gradually from a platelet to an irregular equiaxial shape with increasing Ni concentration. A similarity in WC morphology was found between Fig. 2a and b. With 5% addition of Co–Fe–Ni alloy in Fig. 2b as the binder, the WC phase maintained the platelet shape even when the volume fraction of WC platelets was substantially decreased. The addition of the alloy was intended to resemble the composition of the metallic phase in Fig. 2a. Comparing this to the microstructure of Ni binder (Fig. 2c), Ni is found to cause the irregular equiaxial shape. Assuming that the contribution of dissolved (Ti,W)(CN) to composition is about the same for the systems with different binders, this result suggests that Ni melt tends to reduce the anisotropy of the interface energy of WC more than the Co–Fe–Ni melt at 1510 °C.

The most common crystal shape of WC in WC–Co system is a truncated trigonal prism.[29] However, the shape of WC is sensitive to the binder content and subsequently composition.[30] It is more likely in the systems of this study that the increase in the binder content provides space for WC to grow in and results in different interfacial energies in the system as (Ti,W)(CN) dissolves in the binder. Thus, the change in the WC morphology, with an increase in the binder content, could be due to a different mechanism for the WC platelet formation as explained below.

When the binder content is high, most WC form through the dissolution/precipitation process of (Ti,W)C or (Ti,W)(CN) including initially separated WC. Even though the (Ti,W)(CN) phase is thermodynamically stable, it dissolves in the melt during sintering to reduce the total free energy of the system. In this process $(Ti_{0.6}W_{0.4})(CN)$ and $(Ti_{0.5}W_{0.5})(CN)$ release WC through dissolution and transform to $(Ti_{\sim 0.7}W_{\sim 0.3})(CN)$ as discussed above, which is more stable in the presence of nitrogen. The WC phase released from this dissolution process precipitated and coarsened into an irregular equiaxial shape.

On the other hand, when the liquid binder is scarce, the WC separation is expected to happen by solid-state diffusion in (Ti,W)C or (Ti,W)(CN). The WC separation could be accelerated further in the presence of nitrogen and/or excess W. The separated WC phase would dissolve preferentially and grow on the pre-existing WC along the (Ti,W)(CN) particle boundaries since WC is thermodynamically much less stable than the TiC, Ti(CN) and (Ti,W)C phases.[31,32]

Fig. 3 shows the change in the volume fraction of WC in the $(Ti_{0.6}W_{0.4})C$ and $(Ti_{0.6}W_{0.4})(CN)$ systems sintered at 1510 °C for 1 h. When the Ni content was low (<5 wt%), the influence of nitrogen (5 Torr) on the WC separation was apparent. However, as the Ni content in the binder increased, WC precipitation was facilitated by the dissolution/precipitation process regardless of nitrogen application. This supports the different formation mechanism of the WC platelets with respect to the binder content and nitrogen presence.

3.3. Effect of WC morphology on the mechanical properties

The mechanical properties of the $(Ti_{0.6}W_{0.4})C$ sintered in N_2 were not easy to measure due to high level of porosity. In order to eliminate the residual pores, the samples were pre-sintered under nitrogen flow (30 Torr) and sinter/HIPped. The pre-sintering

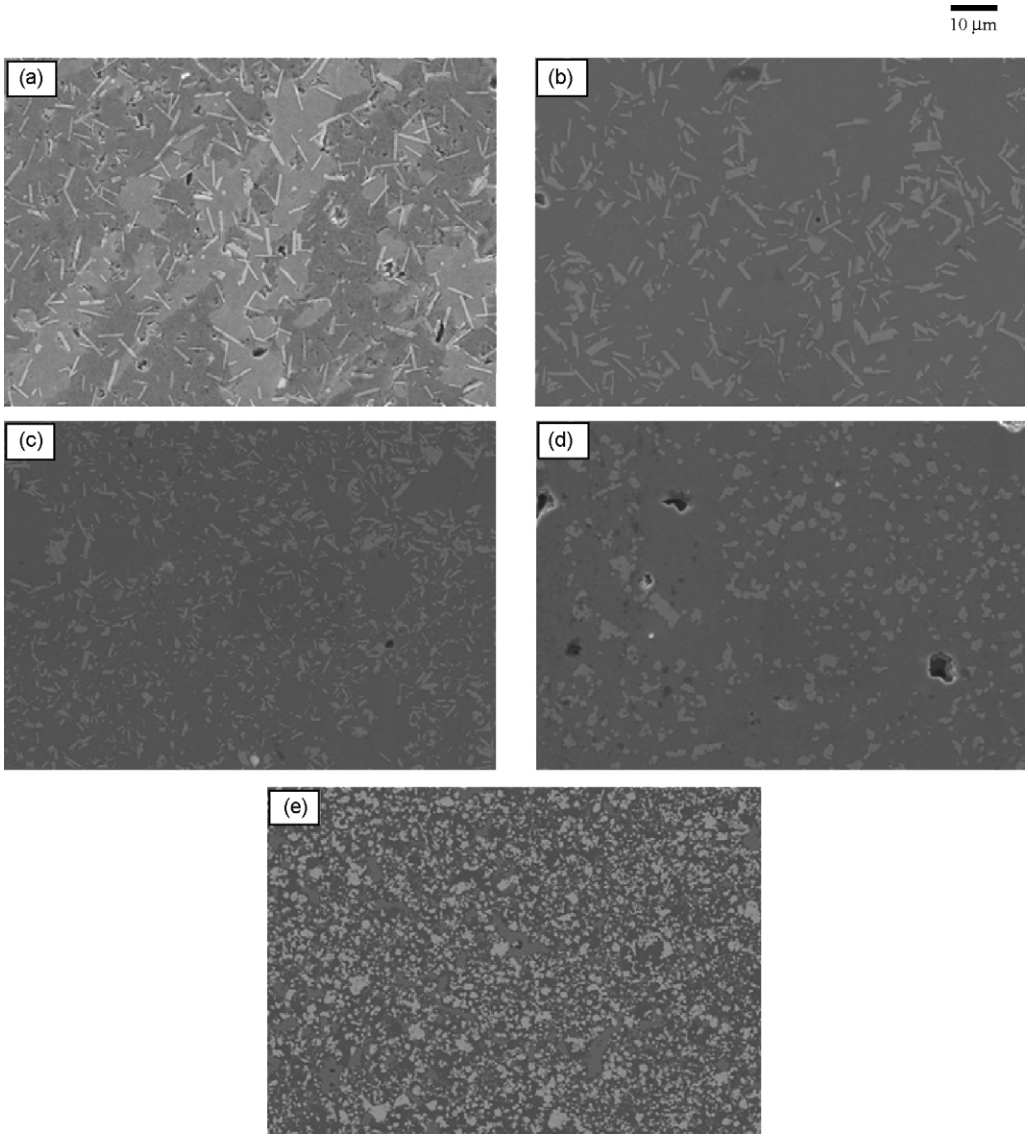

Fig. 2. Microstructure of $(Ti_{0.6}W_{0.4})(CN)$–xMe sintered at 1510 °C for 1 h in N_2 at 5 Torr, where xMe are (a) 0, (b) 5FeCoNi, (c) 5Ni, (d) 10Ni, and (e) 20Ni.

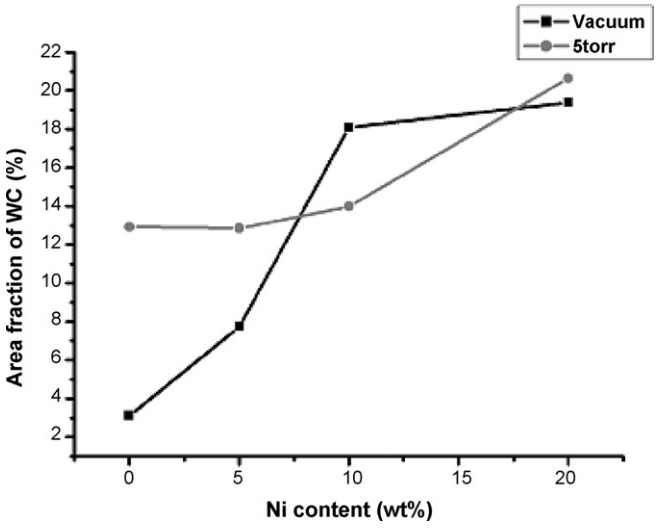

Fig. 3. Volume fraction of WC precipitates in $(Ti_{0.6}W_{0.4})C$- and $(Ti_{0.6}W_{0.4})(CN)$–Ni as a function of binder content.

process formed the WC platelets and the Sinter/HIP process formed fully densified (Ti,W)C with the WC platelets. Table 3 shows Vickers hardness, indentation toughness, and porosity level of the $(Ti_{0.6}W_{0.4})C$ and $(Ti_{0.6}W_{0.4})(CN)$ along with those of advanced structural ceramics and cermets available, which were measured with the same method.[25]

The properties of $(Ti_{0.6}W_{0.4})C$ sintered at 1510 °C in vacuum are excellent (H_v: 18.5–20.0 GPa, K_C: 5.3 MPa $m^{1/2}$) as previously reported.[3] This system contained low concentrations of WC platelets in the microstructure. Interestingly, $(Ti_{0.6}W_{0.4})(CN)$ with WC platelets maintained the level of hardness as that of vacuum sintered $(Ti_{0.6}W_{0.4})C$. Furthermore, the indentation toughness was improved by ~20% from 5.3 to 6.4 MPa $m^{1/2}$. This value was also much superior to other toughened structural ceramics and Ti(CN)-based cermets developed in recent years.[33–37]

Fig. 4 shows the SEM/BSE micrographs of $(Ti_{0.6}W_{0.4})C$ and $(Ti_{0.6}W_{0.4})(CN)$ listed in Table 3. Fig. 4a and b shows the crack tips of indents in (Ti,W)C without WC and (Ti,W)(CN) with WC

Table 3
The mechanical properties of $(Ti_{0.6}W_{0.4})C$ sintered at 1510 °C in vacuum and $(Ti_{0.6}W_{0.4})(CN)$ sinter/HIPed at 1450 °C after pre-sintered at 1350 °C in N_2 30 Torr.

Systems	H_v (GPa)	Indentation toughness (MPa $m^{1/2}$)	Porosity level
$(Ti_{0.6}W_{0.4})C$ (30 kgf)	20.2 (±0.1)	5.3 (±0.1)	A3B1
$(Ti_{0.6}W_{0.4})(CN)$ (30 kgf)	19.3 (±0.6)	6.4 (±0.4)	A1B1
Al_2O_3-SiC[34] (10 kgf)	17.9	3.3	
Si_3N_4–SiC[35] (10 kgf)	16.6	5.2	
Si_3N_4-TiN[36] (20 kgf)	15.0	7.6	
ZrB_2[36] (10 kgf)	18.2 (±0.7)	3.3 (±0.5)	
HfB_2[33] (10 kgf)	21.2 (±0.9)	4.3 (±0.5)	
Ti(CN)-based cermets[37] (10 kgf)	19.4 (±0.8)	3.6 (±0.4)	–

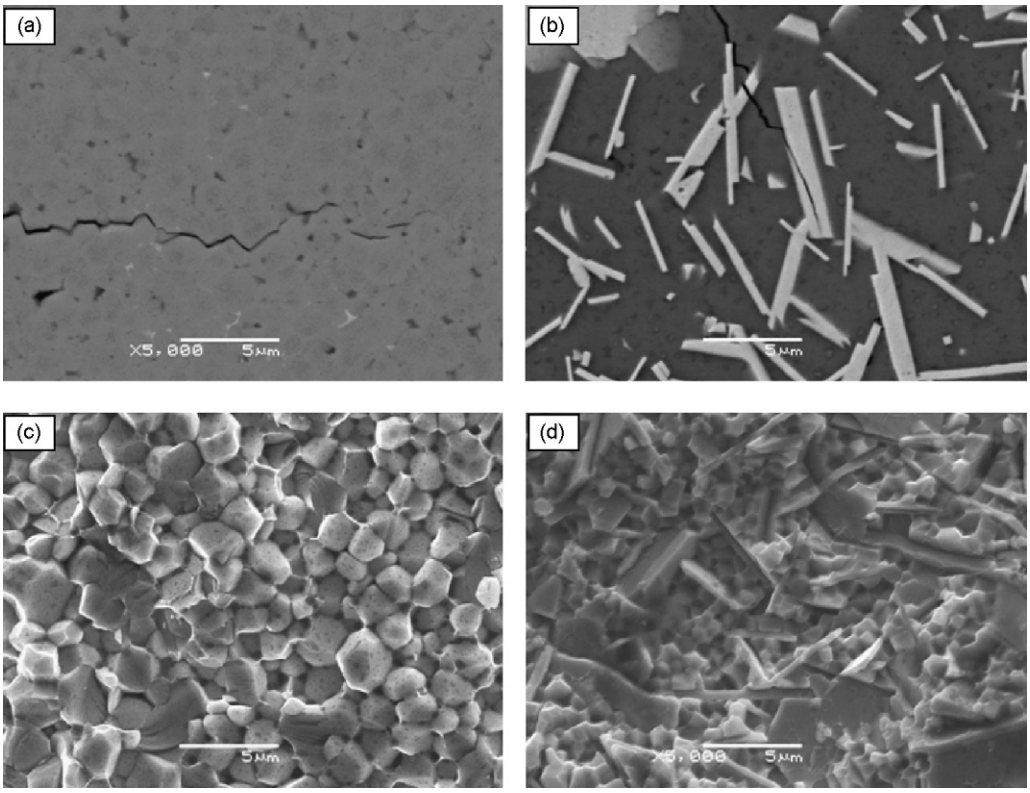

Fig. 4. Crack paths and fracture surfaces of $(Ti_{0.6}W_{0.4})C$ and $(Ti_{0.6}W_{0.4})(CN)$: (a, and c) sintered in vacuum and (b, and d) sinter/HIPed after pre-sintered at 1350 °C in N_2 at 30 Torr.

platelets, respectively. The crack propagates along the (Ti,W)C grain boundaries in Fig. 4a. Pores are frequently found at grain junctions due to insufficient binder. These pores acted as easy crack paths. In the case of (Ti,W)(CN) with the WC platelets (Fig. 4b), the WC phase prevents the propagation of cracks thus toughening the carbides. Crack deflection, bridging, cutting and blunting caused by the WC platelets are anticipated to occur during the fracture process.

Using microstructure analysis of cracks, the dependence of the toughening mechanism and microstructure in toughened ceramics has been found.[38–40] In these analyses toughening mechanism was classified into crack deflection, crack bridging, and cutting elongated grains: 45% were related to crack deflection, 21% to crack bridging, and 34% to cutting among all the WC platelets interacting with cracks. In the $(Ti_{0.6}W_{0.4})(CN)$ system with WC platelets, crack deflection is the principal toughening mechanism and it is related to aspect ratio.[41]

Typical fracture surfaces of (Ti,W)C and (Ti,W)(CN) are shown in Fig. 4c and d, respectively. In the (Ti,W)C sintered in vacuum, intergranular fracture prevailed, which is consistent with Fig. 4a. The grain size of this system was in the range of 1–3 μm. In contrast, the (Ti,W)(CN) sintered in nitrogen shows a facture surface full of WC platelets. Trans- and intergranular fractures dominate due to the presence of WC platelets. This system was exposed to high-temperature sintering twice. Nonetheless, the growth of (Ti,W)(CN) grains was strongly inhibited by the WC platelets, resulting in much smaller grains (~0.5 μm). These small grains might be the cause for the equivalent hardness.

4. Conclusion

In this study, (Ti,W)(CN)-based solid-solution carbides exhibited new microstructures with WC platelets when we

controlled the composition and processing conditions. The separation of WC from (Ti,W)(CN) was ascribed to the solubility limit resulting from the low chemical affinity between nitrogen and W. The morphology of the WC precipitate was affected by the kind and amount of binder phase. With increasing binder content, the WC platelet shape became irregular. This change was attributed not only to surface energy but also to the formation mechanism. A significant improvement in indentation toughness ($K_C \sim 6.4\ \mathrm{MPa\,m^{1/2}}$) was noted in the WC platelet-reinforced (Ti,W)(CN) compared to those of recently reported advanced structural ceramics. It is also notable that the sintering temperature, ~1500 °C, of WC platelet-reinforced (Ti,W)(CN) was much lower than those of advanced structural ceramics, 1700–2000 °C.

Acknowledgements

This work was supported by grants-in-aid for the National Core Research Center Program from MOST/KOSEF (No. R15-2006-022-03001-0) and in part by the basic research fund through KOSEF (No. R01-2008-000-20905-0).

References

1. Zhang, S., Titanium carbonitride-based cermets: process and properties. *Mater. Sci. Eng. A*, 1993, **163**, 141–148.
2. Park, S. and Kang, S., Toughened ultra-fine (Ti,W)(CN)-Ni cermets. *Scr. Mater.*, 2005, **52**, 129–133.
3. Jung, J. and Kang, S., Sintered (Ti,W)C carbides. *Scr. Mater.*, 2007, **56**, 561–564.
4. Park, D. S., Lee, Y. D. and Kang, S., Effect of carbides on the microstructure and properties of Ti(C,N)-based ceramics. *J. Am. Ceram. Soc.*, 1999, **82**, 3150–3154.
5. Xu, C., Ai, X. and Huang, C., Fabrication and performance of an advanced ceramic tool material. *Wear*, 2001, **249**, 503–508.
6. Tashima, S., Yamane, Y., Kuroki, H. and Narutaki, N. J., Cutting performance of high purity alumina ceramic tools formed by a high-speed centrifugal compaction process. *J. Mater. Proc. Technol.*, 1996, **62**, 431–434.
7. Strecker, K., Ribeiro, S., Oberacker, R. and Hoffmann, M. J., Influence of microstructural variation on fracture toughness of LPS-SiC ceramics. *Int. J. Ref. Met. Hard Mater.*, 2004, **22**, 169–175.
8. Liu, X.-J., Huang, Z.-Y., Pu, X.-P., Sun, X.-W. and Huang, L.-P., Influence of planetary high-energy ball milling on microstructure and mechanical properties of silicon nitride ceramics. *J. Am. Ceram. Soc.*, 2005, **88**, 1323–1326.
9. Ren, R. M., Yang, Z. G. and Shaw, L. L., Synthesis of nanostructured TiC via carbothermic reduction enhanced by mechanical activation. *Scr. Mater.*, 1998, **38**, 735–741.
10. Park, S., Kang, Y. J., Kwon, H. J. and Kang, S., Synthesis of (Ti,M1,M2)(CN)–Ni nanocrystalline powders. *Int. J. Refract. Met. Hard Mater.*, 2006, **24**, 115–121.
11. Kwon, H. and Kang, S., Effect of milling on the carbothermal reduction of oxide mixture for (Ti,W)C-Ni. *Mater. Trans.*, 2008, **49**, 1594–1599.
12. Kwon, H. and Kang, S., Carbothermal reduction of titanium monoxide (TiO). *J. Ceram. Soc. Jpn.*, 2008, **116**, 1154–1158.
13. Padture, N. P., In situ-toughened silicon carbide. *J. Am. Ceram. Soc.*, 1994, **77**, 519–523.
14. Ohji, T., Hiral, K. and Kanzaki, S., Fracture resistance behavior of highly anisotropic silicon nitride. *J. Am. Ceram. Soc.*, 1995, **78**, 3125–3128.
15. Li, T., Li, Q., Fuh, J. Y. H., Yu, P. C., Lu, L. and Wu, C. C., Effects of AGG on fracture toughness of tungsten carbide. *Mater. Sci. Eng. A*, 2007, **445–446**, 587–592.
16. Chen, L., Lengauer, W. and Dreyer, K., Advances in modern nitrogen-containing hardmetals and cermets. *Int. J. Refract. Met. Hard Mater.*, 2000, **18**, 153–161.
17. Sommer, M., Schubert, W. D., Zobetz, E. and Warbichler, P., On the formation of very large WC crystals during sintering of ultrafine WC–Co alloys. *Int. J. Refract. Met. Hard Mater.*, 2002, **20**, 41–50.
18. Yoon, B. K., Lee, B. A. and Kang, S. J. L., Growth behavior of rounded (Ti,W)C and faceted WC grains in a Co matrix during liquid phase sintering. *Acta Mater.*, 2005, **53**, 4677–4685.
19. Li, T., Li, Q., Fuh, J. Y. H., Yu, P. C., Lu, L. and Wu, C. C., Effects of lower cobalt binder concentrations in sintering of tungsten carbide. *Mater. Sci. Eng. A*, 2006, **430**, 113–119.
20. Lee, H. R., Kim, D. J., Hwang, N. M. and Kim, D.-Y., Role of vanadium carbide additive during sintering of WC–Co: mechanism of grain growth inhibition. *J. Am. Ceram. Soc.*, 2003, **86**, 152–154.
21. Lay, S., Loubradou, M. and Schubert, W.-D., Structural analysis on planar defects formed in WC platelets in Ti-doped WC–Co. *J. Am. Ceram. Soc.*, 2006, **89**, 3229–3234.
22. Schön, A., Schubert, W. D. and Lux, B., WC platelet-containing hardmetals. In *Proceedings of the 15th International Plansee Seminar*, 2001, pp. 322–336.
23. Brun, M. K., Neguraonkar, R. R. and Stubican, V. S., Precipitation studies in the system WC–TiC. *J. Am. Ceram. Soc.*, 1975, **58**, 392–395.
24. She, Z., A Study on decomposition conditions of TiC–WC solid solutions. *Ref. Met. Hard Mater.*, 1990, **9**, 154–156.
25. Evans, A. G. and Charles, E. A., Fracture toughness determination by indentation. *J. Am. Ceram. Soc.*, 1976, **59**, 371–372.
26. Doi, A., Nomura, T., Tobioka, T. and Takahashi, K., Thermodynamic evaluation of equilibrium nitrogen pressure and WC separation in Ti–W–C–N system carbonitride. In *Proceedings of the 11th International Plansee Seminar*, 1985, pp. 825–843.
27. Jung, J., A study of the formation and thermo-properties of (Ti,W)(CN). *Ph.D. Thesis*, Seoul National University, Korea, 2006.
28. Park, Y. J., Hwang, N. M. and Yoon, D. Y., Abormal growth of faceted (WC) grains in a (Co) liquid matrix. *Metall. Mater. Trans. A*, 1996, **27**, 2809–2819.
29. Lay, S., Allibert, C. H., Christensen, M. and Wahnström, G., Morphology of WC grains in WC–Co alloys. *Mater. Sci. Eng. A*, 2008, **486**, 253–261.
30. Lee, D.-B. and Chae, K.-W., Effect of co additive on the abnormal grain growth of WC. *J. Kor. Ceram. Soc.*, 2004, **41**, 131–135.
31. Ahn, S. Y. and Kang, S., Formation of core/rim structures in Ti(C,N)–WC–Ni cermets via a dissolution and precipitation process. *J. Am. Ceram. Soc.*, 2000, **83**, 1489–1494.
32. Ahn, S. and Kang, S., Dissolution phenomena in the $Ti(C_{0.7}N_{0.3})$–WC–Ni system. *Int. J. Refract. Met. Hard Mater.*, 2008, **26**, 340–345.
33. Baron, B., Kumar, C. S., Le Gonidec, G. and Hampshire, S., Comparison of different alumina powders for the aqueous processing and pressureless sintering of Al_2O_3–SiC nanocomposites. *J. Eur. Ceram. Soc.*, 2002, **22**, 1543–1552.
34. Hwang, K.-T., Kim, C.-S., Auh, K.-H., Cheong, D.-S. and Niihara, K., Influence of SiC particle size and drying method on mechanical properties and microstructure of Si_3N_4/SiC nanocomposite. *Mater. Lett.*, 1997, **32**, 251–257.
35. Zou, B., Huang, C. Z., Liu, H. L. and Chen, M., Preparation and characterization of Si_3N_4/TiN nanocomposites ceramic tool materials. *J. Mater. Proc. Technol.*, 2009, **209**, 4595–4600.
36. Sciti, D., Silvestroni, L. and Nygren, M., Spark plasma sintering of Zr- and Hf-borides with decreasing amounts of $MoSi_2$ as sintering aid. *J. Eur. Ceram. Soc.*, 2008, **28**, 1287–1296.
37. Bellosi, A., Medri, V. and Monteverde, F., Processing and properties of Ti(C, N)–WC-based materials. *J. Am. Ceram. Soc.*, 2001, **84**, 2669–2676.
38. Chou, Y.-S. and Green, D. J., Silicon carbide platelet/alumina composites: III, toughening mechanisms. *J. Am. Ceram. Soc.*, 1993, **76**, 1985–1992.
39. Lee, Y.-I. and Kim, Y.-W., Toughening mechanism in SiC–TiC composites. *J. Ceram. Soc. Jpn.*, 2004, **112**, 18–21.
40. Lee, S.-G., Kim, Y.-W. and Mitomo, M., Relationship between microstructure and fracture toughness of toughened silicon carbide ceramics. *J. Am. Ceram. Soc.*, 2001, **84**, 1347–1353.
41. Becher, P. F., Microstructural design of toughened ceramics. *J. Am. Ceram. Soc.*, 1991, **74**, 255–269.